

## Structured jets and X-ray plateaus in Gamma-ray Bursts

GOR OGANESYAN,<sup>1,2</sup> STEFANO ASCENZI,<sup>1,3</sup> MARICA BRANCHESI,<sup>1,2</sup> OM SHARAN SALAFIA,<sup>4</sup> SIMONE DALL'OSSO,<sup>1</sup> AND GIANCARLO GHIRLANDA<sup>4,5</sup>

<sup>1</sup>*Gran Sasso Science Institute, Viale F. Crispi 7, I-67100, LAquila (AQ), Italy*

<sup>2</sup>*INFN - Laboratori Nazionali del Gran Sasso, I-67100, LAquila (AQ), Italy*

<sup>3</sup>*INAF, Observatory of Abruzzo, Via Mentore Maggini snc, 64100 Collurania, Teramo, Italy*

<sup>4</sup>*INAF - Osservatorio Astronomico di Brera, via Emilio Bianchi 46, I-23807 Merate (LC), Italy*

<sup>5</sup>*INFN - Milano Bicocca, Piazza della Scienza 3, I-20123, Milano, Italy*

### ABSTRACT

The first multi-messenger detection of a binary system of neutron stars, GW170817, brought to the forefront the structured jet model as a way to explain multi-wavelength observations taken over one year. Here we show that high-latitude emission (HLE) from a structured jet can naturally produce an X-ray plateau in gamma-ray burst (GRB) light curves, independent of the radiation from an external shock. We calculate the radiation from a switched-off shell featuring an angular structure in both its relativistic bulk motion and intrinsic luminosity. Our model is able to explain the shallow decay phase (plateau) often observed in GRB X-ray light curves, and its spectral shapes. We discuss the possible contribution of the structured jet HLE to other distinctive features of GRB X-ray light curves, and its capability to explain their observed optical/X-ray temporal behaviour.

### 1. INTRODUCTION

The follow-up of gamma-ray bursts (GRBs) by the X-ray Telescope (XRT, 0.3-10 keV) on board the *Neil Gehrels Swift Observatory* (*Swift* hereafter - Gehrels et al. (2004)) has revealed a rich morphology and diversity in their X-ray counterparts. However, systematic studies of the X-ray light curves have identified a canonical behaviour characterized by the presence of an early steep temporal decay, sometimes followed by a shallow phase at nearly constant flux eventually turning into the characteristic temporal decay expected from an external shock (Nousek et al. 2006; Zhang et al. 2006).

Typically, the steep decay phase ( $F_\nu \propto t^{-\alpha_1}$  with  $3 \leq \alpha_1 \leq 5$ ) lasts up to  $\sim 10^2 - 10^3$  s (Tagliaferri et al. 2005; O'Brien et al. 2006). The shallow decay phase (or “plateau”,  $F_\nu \propto t^{-\alpha_2}$  with  $\alpha_2 \sim 0.5$  or shallower) can extend up to  $\sim 10^4 - 10^5$  s, and it is present for a good fraction of GRBs (Nousek et al. 2006; Zhang et al. 2006; Liang et al. 2007; Willingale et al. 2007). Later, the evolution of the X-ray light curve transitions to a more “canonical” decay ( $F_\nu \propto t^{-\alpha_3}$ , with  $\alpha_3 \sim 1 - 1.5$ ), sometimes showing a further steepening on timescales of a few days. While  $\alpha_3$  is consistent with the temporal slope expected in the standard afterglow model (Sari

et al. 1998), the steep decay and the plateau phases call for a different interpretation.

The initial steep decay phase is often modelled as high-latitude emission (HLE), i.e. the radiation received from larger angles relative to the line of sight, when the prompt emission from a curved surface is switched off (e.g. Liang et al. 2006). It was shown that HLE emission from a spherical surface has a power-law decay  $F_\nu \propto t^{-(\hat{\beta}+2)}$ , where  $\hat{\beta}$  is the slope of the emitted spectrum, typically modelled as a simple power law,  $F_\nu \propto \nu^{-\hat{\beta}}$  (Kumar & Panaitescu 2000). Different modifications of the standard HLE have been considered in previous studies. They include the effects of a finite cooling time (Qin 2008), a non-power law input spectrum (Zhang et al. 2009), time-dependent bulk motion (Uhm & Zhang 2015), a finite size of the emitting shell with multi-pulse contributions (Genet & Granot 2009), an off-axis observer (Lin et al. 2018), and inhomogeneities of the relativistic jet (Dyks et al. 2005; Yamazaki et al. 2006; Takami et al. 2007). While these studies were focused on the effects of jet structure, attention was restricted to the steep decay phase.

The plateau phase instead is usually explained by introducing non-trivial modifications of the standard afterglow theory. The proposed solutions include scenarios with time-varying microphysical parameters of the external shock (Ioka et al. 2006), long-lived reverse shocks (Uhm & Beloborodov 2007; Genet et al. 2007),

delayed afterglow radiation from an in-homogeneous jet (Toma et al. 2006; Eichler & Granot 2006), afterglow radiation in the thick-shell model (Leventis et al. 2014), baryon loading into the external shock from the massive outer shell (Duffell & MacFadyen 2015), delayed onset of the afterglow emission (Kobayashi & Zhang 2007), two-component jet model (Jin et al. 2007) or possible emission prior to the main burst (Yamazaki 2009). Also, prompt emission scattered by dust grains (Shao & Dai 2007) and late-time prompt emission originated from less powerful shells with relatively smaller bulk Lorentz factors (Ghisellini et al. 2007) were proposed as alternative models.

However, the model with the largest consensus considers additional energy injection to the external decelerating shock (Zhang et al. 2006; Granot & Kumar 2006; Nousek et al. 2006, but see, Fan & Piran 2006). The additional energy would prevent the blast wave from decelerating, thus avoiding the typical afterglow decay,  $F \propto t^{-1}$ . The plateau phase, observed up to several  $\times 10^4$  s requires long-lasting activity of the central engine, which can be provided either by the long-term evolution of the accretion disk around a black hole (Kumar et al. 2008; Cannizzo & Gehrels 2009; Lindner et al. 2010) or by the spin-down power released by a newly-born millisecond spinning and highly magnetized neutron star (Zhang & Mészáros 2001; Yu et al. 2010; Metzger et al. 2011; Dall’Osso et al. 2011).

The structured jet (SJ), *i.e.* a jet with an angular profile in both the bulk Lorentz factor and luminosity, has been invoked to explain the multi-wavelength observations of GRB170817A/GW170817 taken over one year (Ghirlanda et al. 2019). Moreover, the SJ enables to explain the overall luminosity function of GRBs (Pescalli et al. 2015). In this work we test the idea that, along with the steep decay, HLE from a SJ can produce the plateau observed in the lightcurve at late times. Qualitatively, the decreasing relativistic beaming of the emission at higher latitudes leads to a shallower light curve with respect to the uniform jet (UJ), for which the bulk Lorentz factor is constant throughout the emitting surface. Furthermore, the latitude-structured bulk motion results in an oblate geometry of the emitting surface which extends the HLE in time. We seek for long-lasting ( $\sim 10^2 - 10^4$  s) flat time-segments in the light curves from HLE arising after  $10^2 - 10^3$  s when the emitting source is switched off.

## 2. HIGH-LATITUDE EMISSION FROM A STRUCTURED JET

We assume an expanding shell in vacuum. As a result of prior interaction with a surrounding medium (the en-

velope of the progenitor star or the ejecta cloud of the progenitor neutron star merger), different parts of the shell move with different velocities. We assume axisymmetry of the velocity relative to the azimuthal angle (in spherical coordinates) and that the observer is perfectly aligned with the center of the shell. At a given time in the rest frame, radiation is produced throughout the entire shell with an infinitesimally short duration.

The adopted model is sketched in Fig. 1: we consider and compare the Uniform Jet model (UJ - red curve) with the Structured jet model (SJ - blue curve). In the UJ model the Lorentz factor is constant along the emitting surface, which is a portion of a sphere. In the SJ case, instead, the Lorentz factor  $\Gamma(\theta)$  decreases with the angular distance from the jet axis,  $\theta$ . This results in a geometry of the emitting surface that differs from a sphere.

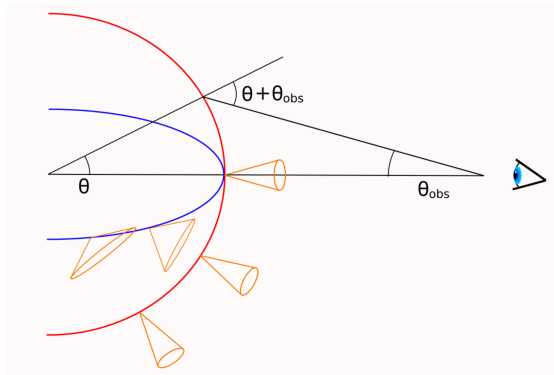


**Figure 1.** Spherical (red) and structured (blue) emitting surfaces corresponding to UJ and SJ, respectively. For the UJ  $\Gamma$  is constant all over the surface, while in the SJ there is an angular dependence which results in the widening of the emitted radiation beaming cone. At a fixed  $\theta$  the travel time of photons in the SJ is longer than in the spherical case. We assume  $\theta + \theta_{obs} \approx \theta$ , *i.e.* we consider distant observers.

The observed flux then depends on the Doppler factor  $\mathcal{D}(\theta) = 1/[\Gamma(\theta)(1 - \beta(\theta) \cos \theta)]$  where  $\beta = v/c$ . In the UJ model (red curve in Fig. 1), the bulk Lorentz factor is constant throughout the shell. This results in a beaming cone with the same angular size  $\sim 1/\Gamma$  for each  $\theta$ . With increasing time, the observer progressively sees the de-beamed emission coming from annuli located at larger angular distances  $\theta$ , causing the monotonical decay of the received flux. In the SJ model (blue curve in Fig. 1), the sharp geometry of the emitting surface causes a slower increase of  $\theta$ , which in turn increases the duration of the HLE. Moreover, the beaming cones corresponding to larger  $\theta$  have increasingly wide beaming angles.

With the assumption that each patch of the shell moves at a constant velocity, we derive the relation between the observed time  $t_{\text{obs}}$  and the angle of the jet  $\theta(t_{\text{obs}})$  from which radiation is received at  $t_{\text{obs}}$ :

$$1 - \frac{\beta(\theta)}{\beta(0)} \cos \theta = \frac{ct_{\text{obs}}}{R_0} \quad (1)$$

where  $R_0$  is the radius of the emitting surface at  $\theta = 0$ . The first photon is assumed to arrive at  $t_{\text{obs}} = 0$  from  $R_0$ .

The observed specific flux is given by the intrinsic spectral shape  $S(\nu')$  and the comoving luminosity  $\epsilon(\theta)$ :

$$F_\nu(t_{\text{obs}}) \propto \mathcal{D}^3(\theta) S(\nu') \epsilon(\theta) \sin \theta \cos \theta |_{\theta(t_{\text{obs}})} \quad (2)$$

where the observer frequency is  $\nu = \mathcal{D}(\theta)\nu'$  (primed quantities are in the comoving frame).

We assume that the intrinsic spectral shape  $S(\nu')$  is angle-independent and we normalize it to 1. For both the UJ and the SJ, the observed flux can be computed by Eq. 2, once the bulk Lorentz factor  $\Gamma(\theta)$ , the comoving luminosity  $\epsilon(\theta)$  and the intrinsic spectral shape  $S(\nu')$  are specified. For a UJ the luminosity is constant throughout the surface.

It is worth noticing that the expression in Eq. 2 integrates over equal arrival time rings, and thus represents a single dimension approximation for the computation of the flux. Considering a finite time duration of the pulse would require integration over equal arrival time surfaces (e.g. see Salafia et al. 2016). However, this results in second order contribution to the observed flux due to finite width of the emitting surface.

### 2.1. The Gaussian structured jet

We adopt a Gaussian jet structure (GJ) for  $\Gamma(\theta)$  and  $\epsilon(\theta)$ , with the same form as in Salafia et al. (2015):

$$\begin{aligned} \epsilon(\theta) &= \epsilon_c e^{-(\theta/\theta_c)^2} \\ \Gamma(\theta) &= 1 + (\Gamma_c - 1) e^{-(\theta/\theta_\Gamma)^2} \end{aligned} \quad (3)$$

where  $\epsilon_c$  and  $\Gamma_c$  are the comoving core luminosity and the bulk Lorentz factor at  $\theta = 0$ , while  $\theta_c$  and  $\theta_\Gamma$  are the jet scaling factors. To compute the observed flux density  $F_\nu(t_{\text{obs}})$ , we adopt a power-law spectral shape  $S(\nu') \propto \nu'^{-\hat{\beta}}$ . The shape of the spectrum influences the temporal behaviour of the HLE since the comoving energy range is blue-shifted by  $\mathcal{D}(\theta)$ , which introduces a spectral dependence in Eq.2.

The shape of the light curve in the GJ case is defined by 5 parameters:  $R_0$ ,  $\Gamma_c$ ,  $\theta_c$ ,  $\theta_\Gamma$ , and the spectral slope  $\hat{\beta}$ . We compute a sequence of light curves with variable parameter sets. For simplicity, we assume  $\theta_c$  equal to  $\theta_\Gamma$ , and set  $\hat{\beta}$  to 1.0, which is the average observed spectral

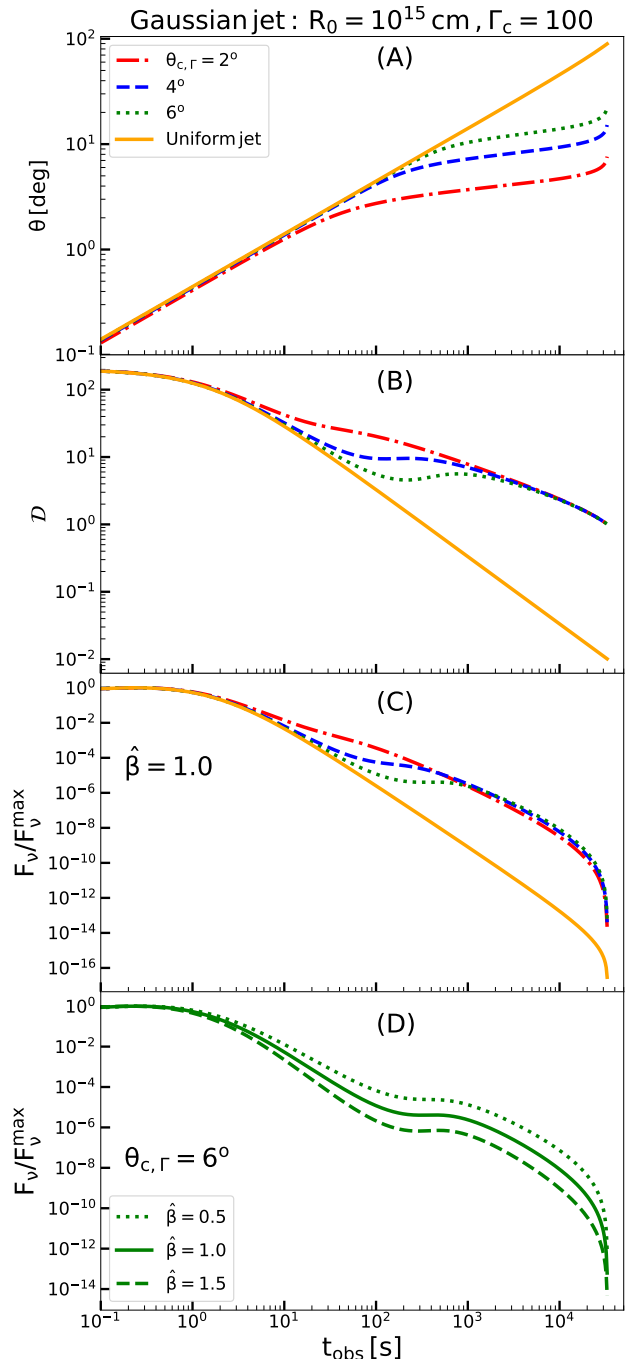


**Figure 2.** Time evolution of the polar angle  $\theta$  of the jet from where radiation is observed (panel A), the corresponding Doppler factor  $\mathcal{D}$  (panel B) and the HLE light curves ( $\hat{\beta} = 1$ , panel C) for the GJ. Colors separate cases with different angular sizes of the jet for the same radial size  $R_0 = 10^{15}$  cm and central bulk Lorentz factor  $\Gamma_c = 100$ . The solid orange lines represent the UJ. The dependence of the light curves from the spectral index  $\hat{\beta}$  is shown in panel D ( $\theta_{c,\Gamma}$  is fixed to  $6^\circ$ ).

index in the plateau phase (Liang et al. 2007). We notice

that flat portions of the light curves can be achieved at relatively late times  $t_{\text{obs}} > 10^2$  s for  $R_0 \geq 10^{15}$  cm,  $\Gamma_c \geq 100$  and  $\theta_{c,\Gamma} \geq 3^\circ$ . We build sequences of light curves by varying each of these three parameters, one at a time, while keeping the other two frozen at the above-mentioned values.

In Fig. 2 we show the time evolution of  $\theta$ ,  $\mathcal{D}$  and the corresponding light-curves for fixed  $R_0 = 10^{15}$  cm and  $\Gamma = 100$ , and three different values of  $\theta_{c,\Gamma}$ . The solution in the UJ case is also reported for reference (solid orange line). The evolution of the polar angle  $\theta$  from where the observer receives photons at a given time is shallower for the SJ (panel A), as a consequence of the oblateness of the emitting surface: the narrower the jet, the longer the time travel difference between photons emitted at different angles. Therefore, the observed time-scale of HLE is longer than in the UJ case. The time evolution of the Doppler factor is affected both by  $\theta(t_{\text{obs}})$  and  $\Gamma(\theta)$  (panel B). On one hand, the decrease of  $\Gamma(\theta)$  with time increases  $\mathcal{D}$  and on the other hand, the increase of  $\theta$  with time reduces  $\mathcal{D}$ . As a result, there is a time-interval where  $\mathcal{D}$  is roughly constant or slightly increasing, while  $\epsilon(\theta)$  is still not decreasing much: this gives rise to the plateau in the light curve (panel C). The deviation of the GJ solution from the UJ case happens essentially at the time when the observer sees the radiation coming from the core border, i.e. when  $\theta = \theta_{c,\Gamma}$ . The peak time of the light curve (i.e. of the prompt pulse) corresponds instead to the time when  $\theta \sim 1/\Gamma_c$ . Panel D shows the light curves assuming different values of  $\hat{\beta}$ , in the range of spectral indices observed during the plateau phase  $0.5 < \hat{\beta} < 1.5$  (Liang et al. 2007). Softer spectra result in steeper decays (as expected in the standard HLE) and fainter plateaus.

We present the solutions of HLE for different sets of parameters  $R_0$  and  $\Gamma_c$  in Fig. 3 (A and B panels). The influence of the size of the jet on the HLE light curve is straightforward: smaller  $R_0$  causes an earlier steep decay (panel A). The dependence of the HLE emission on the bulk Lorentz factor (panel B) shows that the light curves with  $\Gamma_c \geq 500$  present a bump at  $t_{\text{obs}} > t_c$ . This re-brightening can be interpreted as follows: given equal  $\theta_{c,\Gamma}$ , cases with higher  $\Gamma_c$  are characterized by a higher beaming of radiation for  $\theta < \theta_{c,\Gamma}$ . Approaching  $\theta_{c,\Gamma}$  a larger fraction of radiation will be beamed out from the observer, with respect to the low  $\Gamma_c$  case. So, we can expect a higher flux when  $\Gamma_c$  is lower. For  $\theta \gg \theta_\Gamma$  instead, the steep decrease of  $\Gamma(\theta)$ , results in a widening of the beaming angle, which is similar for both the high and low  $\Gamma_c$  cases. Therefore in this picture, the flux emitted by  $\theta \gg \theta_\Gamma$  is almost the same for high and low  $\Gamma_c$ , while the flux emitted for  $\theta \sim \theta_\Gamma$  will suffer a beaming-driven

suppression in the high  $\Gamma_c$  case. As a consequence, the lightcurve characterized by high  $\Gamma_c$  will show the re-brightening, which is however the consequence of the suppression of the flux at earlier times.

The comoving luminosity structure of the jet,  $\epsilon(\theta)$ , additionally suppresses the light curve intensity. The dependence of the light curve shape on  $\epsilon(\theta)$  is much weaker than the dependence on  $\mathcal{D}$ . However, once the Doppler factor drops below 1, the emission becomes de-beamed and the plateau ends. The later very sharp drop is caused by having reached the edge of the jet.

## 2.2. Power-law structured jet

We compute HLE from the power-law jet structure (PJ) for  $\epsilon(\theta)$  and  $\Gamma(\theta)$  adopted from Salafia et al. (2015):

$$\epsilon(\theta) = \begin{cases} \epsilon_c & \theta \leq \theta_c \\ \epsilon_c (\theta/\theta_c)^{-k} & \theta > \theta_c \end{cases} \quad (4)$$

$$\Gamma(\theta) = \begin{cases} \Gamma_c & \theta \leq \theta_\Gamma \\ 1 + (\Gamma_c - 1) (\theta/\theta_\Gamma)^{-k} & \theta > \theta_\Gamma \end{cases}$$

where  $\epsilon_c$  and  $\Gamma_c$  are the comoving luminosity and the bulk Lorentz factor at  $\theta = 0$ ,  $\theta_c$  and  $\theta_\Gamma$  are the jet scaling factors and  $k$  is the slope of the power-law tail, i.e. the steepness of the jet structure.

We compute the observed flux density  $F_\nu(t_{\text{obs}})$  using a power-law spectrum  $S(\nu') \propto \nu'^{-\hat{\beta}}$  with  $\hat{\beta} = 1.0$ . In the Fig. 4 we show the time evolution of  $\theta$  (panel A),  $\mathcal{D}$  (panel B) and the corresponding light-curves for  $R_0 = 10^{15}$  cm,  $\Gamma = 100$ ,  $k = 2$  and  $\theta_{c,\Gamma}$  varying in the range between  $2^\circ$  and  $6^\circ$  (panel C). We present also HLE from the UJ (solid orange line). Similarly to the GJ solutions, we show the dependence of the light curves on the spectral index  $\hat{\beta}$  in panel D. One can notice that the rise of  $\theta$  is faster compared to the GJ case. This is simply due to the shallower angle dependence of  $\Gamma(\theta) \propto \theta^{-2}$  than in GJ. The Doppler factor deviates from the UJ case at times  $t_{\text{obs}} > t_c$  (post-core): the smaller the core size of the jet, the earlier is the slowing down of the  $\mathcal{D}(t_{\text{obs}})$  variation. The major difference of  $\mathcal{D}(t_{\text{obs}})$  compared to the GJ case is that the post-core temporal decay is monotonic, contrary to the ‘‘bumpy’’ trend of the GJ (see panel B of Fig. 2). The plateau phase is more prominent and longer (up to  $10^4$  s) in the PJ case. The fast rise of  $\theta(t_{\text{obs}})$  results in the sharp decay phase at the end of the plateau.

We present the solutions of HLE from the PJ for variable set of parameters in Fig. 3 (panels C-E). In panel C we show the effect of  $R_0$  on the HLE. Differently from the GJ, the light curves have more prominent flat segments that start at later times with an increase of  $R_0$ .

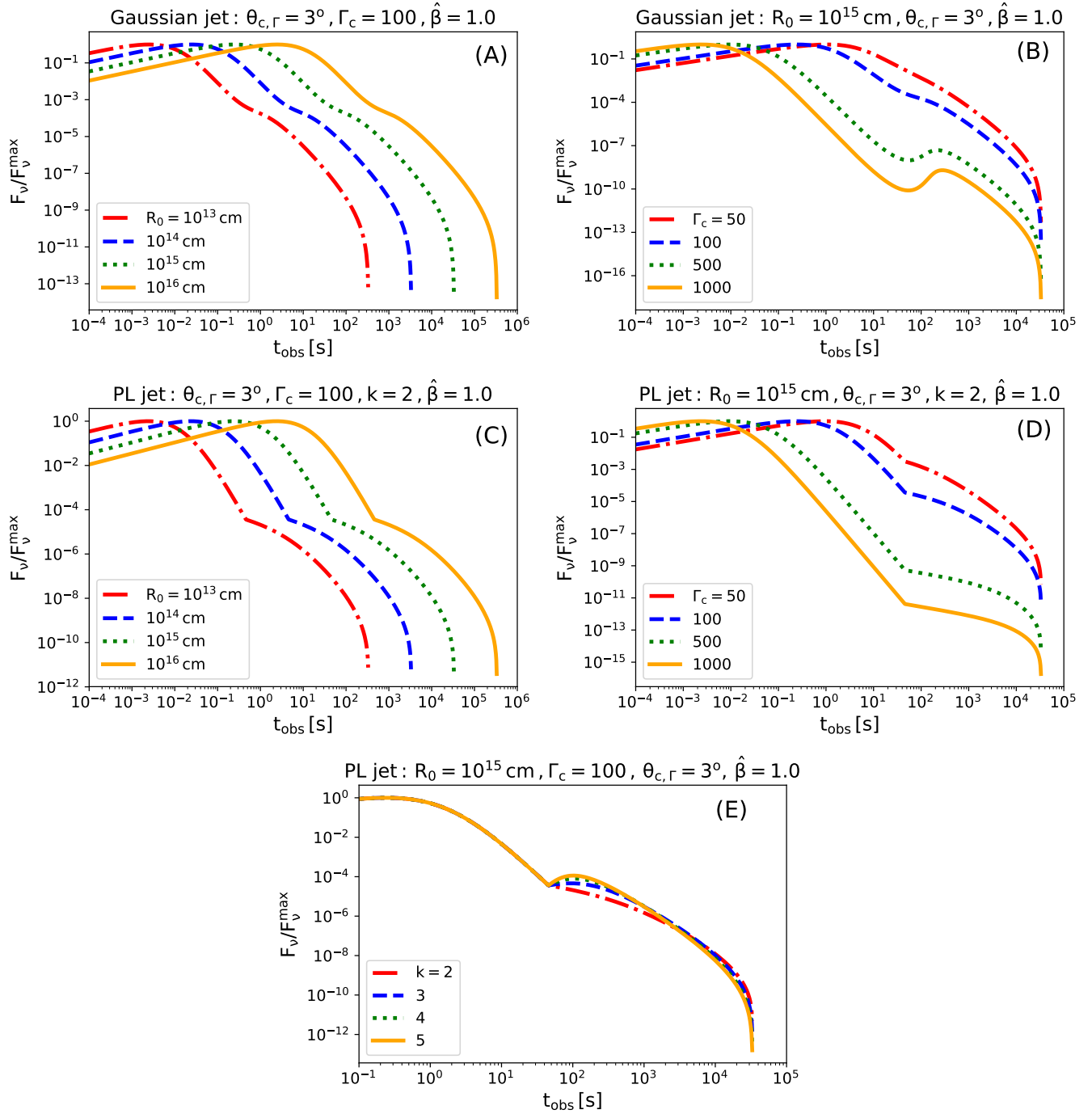


**Figure 3.** HLE light curves from Gaussian and power-law structured jets for different sets of parameters.

Moreover, the post-plateau sharp decay appears earlier due to the faster rise of  $\theta(t_{\text{obs}})$ . We show the HLE parameters and light curves dependence from  $\Gamma_c$  in panel D. One can notice that the plateau phase is flatter with an increase of  $\Gamma_c$ . Moreover, the duration of the plateau phase exceeds  $t_{\text{obs}} \sim 10^4$  s. The flat and long plateau is provided by the shallow jet structure i.e.  $k = 2$  which causes an extremely fast rise of  $\theta(t_{\text{obs}})$ . The increase of

$k$  results in re-brightening of the light curve (see panel E). The origin of the re-brightening for higher  $k$  is due to the fact that a steeper jet structure leads to a faster widening of the beaming angle. This results in a higher fraction of radiation reaching the observer at post-core time.

### 3. TESTING PREDICTIONS OF THE HLE MODEL

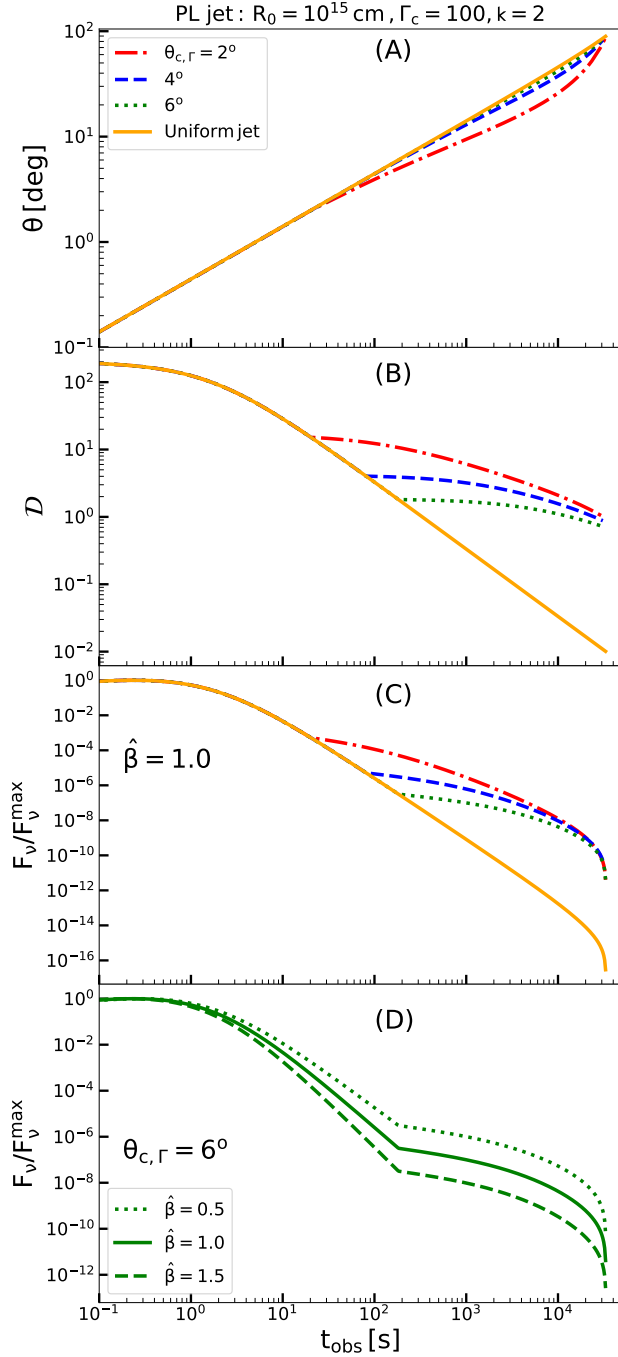


**Figure 4.** Time evolution of the polar angle  $\theta$  of the jet from where radiation is observed (panel A), the corresponding Doppler factor  $\mathcal{D}$  (panel B) and the HLE light curve ( $\hat{\beta} = 1$ , panel C) for the power-law structured jet. Colors separate cases with different angular sizes of the jet for the same radial size  $R_0 = 10^{15}$  cm, central bulk Lorentz factor  $\Gamma_0 = 100$  and power-law index  $k=2$ . The solid orange lines represent the UJ. The dependence of the light curves from the spectral index  $\hat{\beta}$  is shown in panel D ( $\theta_{c,\Gamma}$  is fixed to  $6^\circ$ ).

We aim to test the ability to match the temporal and spectral properties of the X-ray plateau by our toy model.

### 3.1. Theoretical light curve and GRB 061121

As an illustration, we compare our model calculations with the X-ray light curve of GRB 061121. The choice of this particular GRB is motivated by several requirements:

- Presence of the fast decay and plateau phases in the X-ray light curve.
- Relatively bright GRB in order to best meet the assumption of an “on-axis” observer.
- Spectral information on the brightest pulse in the prompt emission extending to the X-rays. Because each pulse of the prompt emission produces HLE, the brightest pulse is expected to provide the dominant contribution to the plateau emission. Spectral information in the X-ray band allows us to fix the source spectrum before it is switched off.

The left panel of Fig. 5 shows the multi-band light curve of GRB 061121, observed simultaneously by *Swift*/BAT (15-150 keV), XRT, and *Swift*/UVOT in the white filter (Page et al. 2007). The peak time of the main prompt pulse at  $t_0 \sim 74$  s (indicated by the grey vertical line) is chosen as time zero for our model, *i.e.*, we assume the emitting source is switched off at  $t_0$ . The optical (green points) and X-ray (black points) light curves are time-shifted ( $t_{\text{obs}} = t - t_0$ ) in the right panel of Fig. 5.

The joint XRT and BAT time-resolved spectra of GRB 061121 have been modelled as a broken power-law (Page et al. 2007; Oganessian et al. 2017). Recent studies have pointed out that broad-band prompt emission spectra of GRBs can generally be fitted by a double broken power-law model (2BPL) with low-energy spectral indices consistent with synchrotron radiation (Oganessian et al. 2017, 2018; Ravasio et al. 2018, 2019). Therefore, we adopt 2BPL for the prompt emission pulse (at its peak) to model HLE. The photon indices below and above the low-energy break at  $E_{\text{break}}$  are  $\alpha_1 = -2/3$  and  $\alpha_2 = -1.5$  which correspond to spectral indices  $\beta_1 = -1/3$  and  $\beta_2 = 0.5$  in  $F_\nu \propto \nu^{-\hat{\beta}}$  representation. The spectrum around the peak time of the prompt pulse ( $t_0$ ) is best fitted with  $E_{\text{break}} \sim 2.5$  keV (Oganessian et al. 2017). We use this value as an input for modelling the HLE in the XRT spectral range. The corresponding break energy in the comoving frame is then  $E_{\text{break}}/\mathcal{D}(\theta = 0)$ . Furthermore, we assume the peak energy (*i.e.* that of the higher energy break in the 2BPL

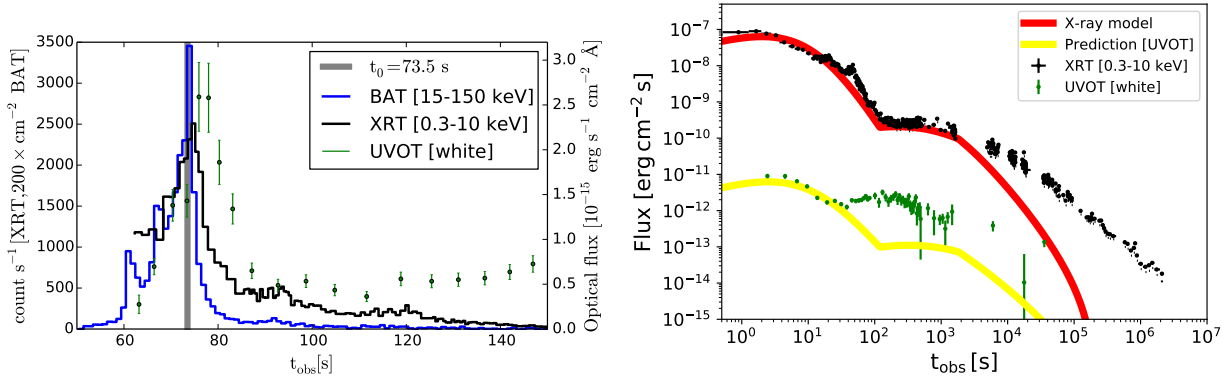


**Figure 5.** Left panel: joint BAT (blue), XRT (black) and optical (green) lightcurve of GRB 061121 for the brightest prompt emission pulse. The gray vertical line indicates the peak time of the prompt emission  $t_0$  used as a reference time for modelling HLE. Right panel: X-ray flux (0.3-10 keV, in black) modeled by HLE with PJ (red) and HLE prediction in the optical domain (yellow) in comparison with *Swift*/UVOT data points.

model)  $E_{\text{peak}} > 150$  keV since it is not constrained by BAT data. However, we have verified that its exact value does not affect the X-ray light curve at the observed time of the plateau.

To reproduce the fast decay and the plateau phase observed in the X-ray emission (at 0.3-10 keV) of GRB 061121 using the HLE model, we adopt a PJ with  $\Gamma_c = 100$ ,  $R_0 = 5.5 \times 10^{15}$  cm,  $\theta_c = 6^\circ$ ,  $\theta_\Gamma = 2^\circ$  and  $k = 2$  (red line in the left panel of Fig. 5). Keeping the same parameters, we compute the corresponding HLE emission in the white UVOT filter energy range. The predicted light curve (yellow line in the right panel of Fig. 5) accounts well for the early decrease in flux. The later bump at  $t \sim 10^2 - 10^3$  s suggests the rising of a new emission component, which we can attribute to the external shock. This late component could also explain the X-ray lightcurve beyond the end of the plateau, where the HLE fades rapidly while the XRT flux shows a much more gradual decay. This example illustrates the role of HLE in shaping GRB lightcurves: an additional component of the prompt emission, particularly important in the X-ray range, which naturally produces a steep decay followed by a longer-lasting plateau as a consequence of a generic jet structure.

### 3.2. Spectral properties of the HLE plateau

Predictions of the HLE model extend to the spectral properties of GRB X-ray counterparts because, if the X-ray emission is dominated by HLE, then its spectrum is the same as the prompt. Therefore, assuming the comoving spectrum is the same at all angles  $\theta$ , the decrease of  $\mathcal{D}$  with time means that the observer is probing a progressively higher energy part of the prompt emission spectrum, since the observed photon energy is  $E_{\text{obs}} = E' \mathcal{D}$  ( $E'$  being the corresponding comoving energy). Let us assume a typical  $\Gamma_c \sim 100$ : for the GJ, our

solutions from the previous section indicate that  $\mathcal{D} \sim 10$  at the start of the plateau. Therefore, the spectral index in the plateau phase (at  $\sim 10$  keV) would correspond to that at around  $\sim 100$  keV in the prompt emission pulse at  $t_0$ . The latter is close to the typical peak energy of the prompt emission spectrum ( $\sim 200$  keV; e.g. Nava et al. 2011). Therefore, the photon index in the plateau phase can vary between  $-1.5$ , the spectral slope below  $E_{\text{peak}}$ , and  $\hat{\beta}_p$  which is the photon index above  $E_{\text{peak}}$ . The value of  $\hat{\beta}_p$  ranges between  $-2$  and  $-3$  (e.g. Nava et al. 2011) which is consistent with the spectral analysis of the plateau phase (Liang et al. 2007) suggesting a range of photon indices between  $-1.5$  and  $-2.5$ .

## 4. CONCLUSIONS

We studied the high-latitude emission (HLE) arising from the abruptly switched off pulse of a relativistic jet with an angular structure in bulk motion and comoving luminosity. Using both Gaussian (GJ) and power-law (PJ) jet structures, we tested predictions of this model using the joint X-ray and optical light curve of GRB 061121. Our results can be summarized as follows:

- The plateau phase observed in a good fraction of X-ray GRB lightcurves can arise from the HLE of a structured jet. Plateaus starting at  $t_{\text{obs}} \sim 10^2 - 10^3$  s require that the size of the jet at prompt emission to be  $R_0 \gtrsim 10^{15}$  cm. While in the GJ model only plateau durations of  $\sim 10^3$  s can be obtained, the PJ model can provide more extended plateaus (up to  $\sim 5 \times 10^4$  s).
- The post-plateau phase in the HLE model with a jet structure is characterized by two further segments of flux decay: a power-law followed by a very sharp drop. The latter could provide a novel

explanation for such puzzling features observed in some GRB X-ray lightcurves (e.g. Troja et al. 2007).

- The spectra of the plateau phase in the X-ray energy range are consistent with the HLE predictions. In particular, measured photon indices ( $-2.5 < \alpha < -1.5$ , Liang et al. 2007) are in agreement with the synchrotron model for the prompt emission. The spectral softening typically observed in the steep-decay/plateau transition is also naturally explained in our model.

Previous studies of HLE from inhomogeneous jets (Dyks et al. 2005; Yamazaki et al. 2006; Takami et al. 2007) were focused on the influence of jet structure on the fast decay phase. The flattening of HLE at  $\sim 30$  s due to the bulk motion structure has been noticed previously in Dyks et al. (2005). However, these authors did not obtain solutions for the plateau phase observed at  $\sim 10^2 - 10^3$  s. This is due to the limited parameter space considered in their work, e.g. the size of the jet, fixed to  $R_0 \sim 10^{14}$  cm.

We have shown that the HLE from a structured jet is able to explain the complex morphology of X-ray counterparts of GRBs, including fast decay, plateau and post-plateau phases. The systematic application of this model to optical-to-X-ray data will provide a mean of probing the angular structure of GRB jets and the size of the emitting region during the prompt emission. A thorough exploration of these aspects will be the subject of subsequent works.

GO would like to thank Gabriele Ghisellini and Elias S. Kammoun for fruitful discussions. GO and SA are thankful to INAF – Osservatorio Astronomico di Brera for kind hospitality during the completion of this work. SA acknowledges the GRAvitational Wave Inaf TeAm - GRAWITA (P.I. E. Brocato). This work made use of data supplied by the UK Swift Science Data Centre at the University of Leicester.

## REFERENCES

- Cannizzo, J. K., & Gehrels, N. 2009, *ApJ*, 700, 1047
- Dall’Osso, S., Stratta, G., Guetta, D., et al. 2011, *A&A*, 526, A121
- Duffell, P. C., & MacFadyen, A. I. 2015, *ApJ*, 806, 205
- Dyks, J., Zhang, B., & Fan, Y. Z. 2005, arXiv e-prints, astro
- Eichler, D., & Granot, J. 2006, *ApJL*, 641, L5
- Fan, Y., & Piran, T. 2006, *MNRAS*, 369, 197
- Gehrels, N., Chincarini, G., Giommi, P., et al. 2004, *ApJ*, 611, 1005
- Genet, F., Daigne, F., & Mochkovitch, R. 2007, *MNRAS*, 381, 732
- Genet, F., & Granot, J. 2009, *MNRAS*, 399, 1328
- Ghirlanda, G., Salafia, O. S., Paragi, Z., et al. 2019, *Science*, 363, 968
- Ghisellini, G., Ghirlanda, G., Nava, L., & Firmani, C. 2007, *ApJL*, 658, L75
- Granot, J., & Kumar, P. 2006, *MNRAS*, 366, L13
- Ioka, K., Toma, K., Yamazaki, R., & Nakamura, T. 2006, *A&A*, 458, 7
- Jin, Z. P., Yan, T., Fan, Y. Z., & Wei, D. M. 2007, *ApJL*, 656, L57
- Kobayashi, S., & Zhang, B. 2007, *ApJ*, 655, 973
- Kumar, P., Narayan, R., & Johnson, J. L. 2008, *Science*, 321, 376
- Kumar, P., & Panaitescu, A. 2000, *ApJ*, 541, L51
- Leventis, K., Wijers, R. A. M. J., & van der Horst, A. J. 2014, *MNRAS*, 437, 2448
- Liang, E.-W., Zhang, B.-B., & Zhang, B. 2007, *ApJ*, 670, 565
- Liang, E. W., Zhang, B., O’Brien, P. T., et al. 2006, *ApJ*, 646, 351
- Lin, D.-B., Liu, T., Lin, J., et al. 2018, *ApJ*, 856, 90
- Lindner, C. C., Milosavljević, M., Couch, S. M., & Kumar, P. 2010, *ApJ*, 713, 800
- Metzger, B. D., Giannios, D., Thompson, T. A., Bucciantini, N., & Quataert, E. 2011, *MNRAS*, 413, 2031
- Nava, L., Ghirlanda, G., Ghisellini, G., & Celotti, A. 2011, *A&A*, 530, A21
- Nousek, J. A., Kouveliotou, C., Grupe, D., et al. 2006, *ApJ*, 642, 389
- O’Brien, P. T., Willingale, R., Osborne, J., et al. 2006, *ApJ*, 647, 1213
- Oganesyan, G., Nava, L., Ghirlanda, G., & Celotti, A. 2017, *ApJ*, 846, 137
- . 2018, *A&A*, 616, A138
- Page, K. L., Willingale, R., Osborne, J. P., et al. 2007, *ApJ*, 663, 1125
- Pescalli, A., Ghirlanda, G., Salafia, O. S., et al. 2015, *MNRAS*, 447, 1911
- Qin, Y. P. 2008, *ApJ*, 683, 900

- Ravasio, M. E., Ghirlanda, G., Nava, L., & Ghisellini, G. 2019, arXiv e-prints, arXiv:1903.02555
- Ravasio, M. E., Oganessian, G., Ghirlanda, G., et al. 2018, *A&A*, 613, A16
- Salafia, O. S., Ghisellini, G., Pescalli, A., Ghirlanda, G., & Nappo, F. 2015, *MNRAS*, 450, 3549
- Salafia, O. S., Ghisellini, G., Pescalli, A., Ghirlanda, G., & Nappo, F. 2016, *MNRAS*, 461, 3607
- Sari, R., Piran, T., & Narayan, R. 1998, *ApJ*, 497, L17
- Shao, L., & Dai, Z. G. 2007, *ApJ*, 660, 1319
- Tagliaferri, G., Goad, M., Chincarini, G., et al. 2005, *Nature*, 436, 985
- Takami, K., Yamazaki, R., Sakamoto, T., & Sato, G. 2007, *ApJ*, 663, 1118
- Toma, K., Ioka, K., Yamazaki, R., & Nakamura, T. 2006, *ApJL*, 640, L139
- Troja, E., Cusumano, G., O'Brien, P. T., et al. 2007, *ApJ*, 665, 599
- Uhm, Z. L., & Beloborodov, A. M. 2007, *ApJL*, 665, L93
- Uhm, Z. L., & Zhang, B. 2015, *ApJ*, 808, 33
- Willingale, R., O'Brien, P. T., Osborne, J. P., et al. 2007, *ApJ*, 662, 1093
- Yamazaki, R. 2009, *ApJL*, 690, L118
- Yamazaki, R., Toma, K., Ioka, K., & Nakamura, T. 2006, *MNRAS*, 369, 311
- Yu, Y.-W., Cheng, K. S., & Cao, X.-F. 2010, *ApJ*, 715, 477
- Zhang, B., Fan, Y. Z., Dyks, J., et al. 2006, *ApJ*, 642, 354
- Zhang, B., & Mészáros, P. 2001, *ApJL*, 552, L35
- Zhang, B.-B., Zhang, B., Liang, E.-W., & Wang, X.-Y. 2009, *ApJ*, 690, L10